DETERMINATION OF MODE II TRACTION SEPARATION LAW FOR S-2 GLASS/EPOXY INTERFACE UNDER DIFFERENT LOADING RATES USING A MICRODROPLET TEST METHOD

Sandeep Tamrakar[1, 3*], Raja Ganesh[1, 4], Subramani Sockalingam[1,4,5], John W. Gillespie Jr.[1, 2, 3, 4]

[1] Center for Composite Materials (UD-CCM)
[2] Department of Materials Science & Engineering
[3] Department of Civil & Environmental Engineering
[4] Department of Mechanical Engineering
University of Delaware, Newark, DE 19716

[5] Current address: Department of Mechanical Engineering, University of South Carolina, Columbia SC 29201

*Corresponding author. Tel.: +1(302) 831-6644 (Sandeep Tamrakar)
Email address: tamrakar@udel.edu

ABSTRACT

This paper presents a methodology to extract the rate dependent traction separation law for composite interface through iterative method by simulating all the physically observed mechanisms in a microdroplet experiment. Experimentally obtained rate dependent interfacial shear strength (1 µm/s to 1 m/s), large strain resin properties (0.001/s to 12,000/s) and information on crack initiation at the interface obtained from carbon nanotube sensors are used as model input. Through simulation of microdroplet experiments, unique set of traction separation laws were determined for a given loading rate by narrowing down the range based on IFSS prediction for different droplet sizes and the associated failure modes Both traction law parameters, i.e. peak traction and the fracture energy increase with the increase in the rate of loading. Partitioning of energy absorption contribution by the constituents suggests resin plasticity and strain energy stored in the fiber play an important role up to failure.

Keywords: traction law, composite interface, microdroplet, S-2 glass/epoxy

1. Introduction

In the automotive industry, there is a demand for lightweight composite structure with enhanced energy dissipation capability during an event of crash or impact. Under dynamic loading, energy is dissipated through various mechanism such as delamination, matrix cracking at higher length scale and fiber matrix debonding, frictional sliding and fiber breakage at lower length scale. Studies have shown that the damage mechanisms pertaining to lower length scales absorb more energy [xx]. The interaction between fiber and matrix at the interface determines the overall energy absorption capability of the fiber reinforced composite material [1]. A coating on the surface of the fiber called sizing, which is in the nanometer length scale, consists of film former and silane coupling agents [2,3]. The chemical formulation of the sizing and its compatibility with the resin significantly affects the degree of adhesion between fiber and matrix and ultimately the energy absorbing capability of the composite [4,5]. This opens an opportunity to maximize the composite properties by studying the energy dissipation and failure mechanisms during interface debonding and design lightweight automotive parts. An ideal case for maximum energy absorption would be to have resin deform plastically near the interface with the ultimate failure occurring along the interface. Since this is a dynamic event, it become important to consider the rate dependent properties of the matrix as well as the interface.

One approach to optimize the interaction between constituents for maximum energy absorption is by studying a model composite through finite element simulation (FEA). This requires accurate rate dependent properties for fiber, resin and interface. In FEA simulation, cohesive zone models are generally used to simulate the interface between two dissimilar materials. Dependence of traction law parameters on the rate of loading has been reported in the literature [6–8]. For instance, traction law obtained through direct approach for steel adherends bonded with polyurea exhibited strong dependence on the rate of loading [8]. Rahulkumar et al. [9] modeled fracture in viscoelastic materials by combining viscoelastic adhesive model with a rate independent cohesive zone model. Xu et al. [10] modeled rate dependent failure behavior of adhesive bonds by introducing a Maxwell element to a rate independent cohesive zone model. Model parameters were determined by simulating DCB tests conducted at different strain rates. Wang et al. [11] employed spring and dashpots to introduce viscoelastic factor in the cohesive zone model and simulated DCB tests with metal adhesive (elastic) and rubber adhesive (hyperelastic) structure. Marzi et al. [12] used a rate dependent extension of bilinear cohesive model and implemented in commercial FE code LS-DYNA via a user-defined subroutine. Butt joint and tapered DCB tests were conducted at velocities ranging from 10^{-2} mm/s to 10^{2} mm/s to determine the Mode I model parameters. Gowrishankar et al. [7] adopted an iterative approach in which the toughness of silicon/epoxy interface was estimated by comparing the crack length in a DCB specimen, and then the peak traction was adjusted to match the experimental results. These parameters were in good agreement with the ones extracted directly.

In this study, traction law parameters are iteratively determined by accurately simulating and matching the experiments [13,14]. This route, in conjunction with the novel test methods developed for characterization of rate dependent interface and resin properties in our previous studies [15,16] and in-situ sensing of crack initiation, is the approach used.

2. Microdroplet test

S-2 glass fibers with (3-glycidoxypropyl) trimethoxy silane coupling agent and epoxy film former sizing obtained from Owens Corning Corporation were used. Epoxy resin DER 353 (Dow Chemical Company) was mixed with bis (p-aminocyclohexyl) methane (PACM-20) curing agent (Air Products and Chemicals, Inc.) at stoichiometric ratio of 100:28 (weight ratio) to form the droplets which is then allowed to gel at room temperature for 5 h, followed by curing at 80 and 150 °C for 2 h each. At least 10 valid microdroplet tests were used for each loading rate. The nominal diameter of the S-2 glass fibers considered in this study was 10 μm. The embedded length of the droplet ranged from 70 to 200 μm. Fiber gauge lengths (top of drop to load cell) between 1 mm and 2 mm were maintained. Tests were conducted at 1 um/s, 0.1 mm/s and 1 m/s [17]. A modified tensile Hopkinson bar was used for 1 m/s loading rate. Details on this test setup can be found in [15].

Experimental results exhibited size effects showing lower IFSS for higher embedded length, which are accounted for in the simulation. The average IFSS increased by a factor of 1.6 when the displacement rate was increased from 1 μm/s to 1 m/s (See Figure 1 and Table 1). Resin plasticity in the droplet is observed at the location of knife edge contact. Finite element simulation of the microdroplet experiments incorporates accurate rate dependent resin properties to partition the resin and interface energy contributions.

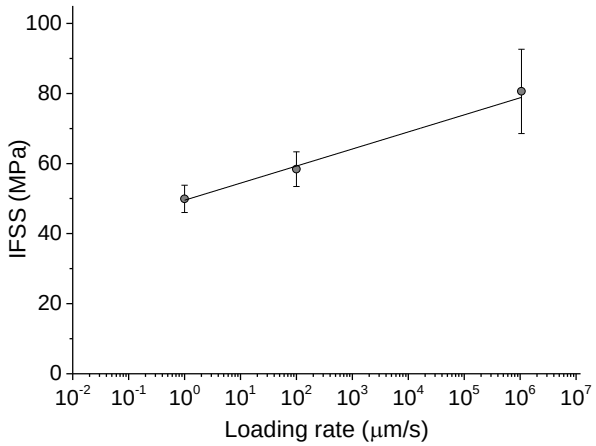

Figure 1 Average IFSS vs. loading rate for microdroplet specimens with embedded length ranging from 70 μm to 125 μm show a linear increase when plotted on a log scale

Table 1 Rate dependent IFSS and specific energy up to debond

Loading Rate	IFSS (MPa)	Specific energy debond (J/m^2)
1 µm/s	49.9 ± 4.7	670 ± 220
0.1 mm/s	58.4 ± 4.9	880 ± 350
1 m/s	80.6 ± 12.1	1950 ± 860

3. Proposed methodology for the determination of traction separation law

Our proposed methodology to determine rate dependent traction separation law for composite interfaces includes characterizing the rate dependent response of fiber, matrix and interface separately. Then, by accurately simulating all the physically observed mechanisms in the specimen, unique traction law can be determined. Parametric studies on a bilinear traction law conducted by Tamrakar et al. [24] demonstrated a non-unique nature of the traction law where there are more than one combinations of peak traction and relative displacement for crack separation traction law parameters that accurately predict the maximum load. Two different combinations of peak traction and fracture energy resulted in very similar force displacement response. However, the point at which crack initiation occurs varies. For the traction law with 160 J/m^2 and 120 MPa peak traction, the crack initiates at around 88% of the peak load, whereas for the one with 200 J/m2 and 75 MPa, crack initiation occurs right after reaching the peak load. These parametric studies suggest that additional experimental information such as load at the initiation of debonding along the interface is important to establish uniqueness. For this purpose, the authors developed CNT sensors at sub-micron length scale to monitor the onset of crack initiation at the interface, where the CNT sensors act as on/off switch [17]. Measurements on change in electrical resistance during microdroplet test showed that the crack initiation occurs at the peak load and becomes unstable and failure occurs. Information on crack onset and its corresponding load level is used as an input in the FE simulation to extract traction separation law.

Resin plasticity is another factor that that must be accounted for in simulations of the microdroplet experiments for accurate traction law determination. During the experiments, large plastic deformation has been observed at the tip of the droplet where knife edge comes in contact. When only the elastic response of the resin is considered, interface debonding is assumed to be the only energy absorption mechanism. However, when resin yield stress is exceeded additional energy absorption occurs through resin plasticity. Rate dependent yield stress and stress strain response for DER 353 epoxy resin serve as input in the model [17].

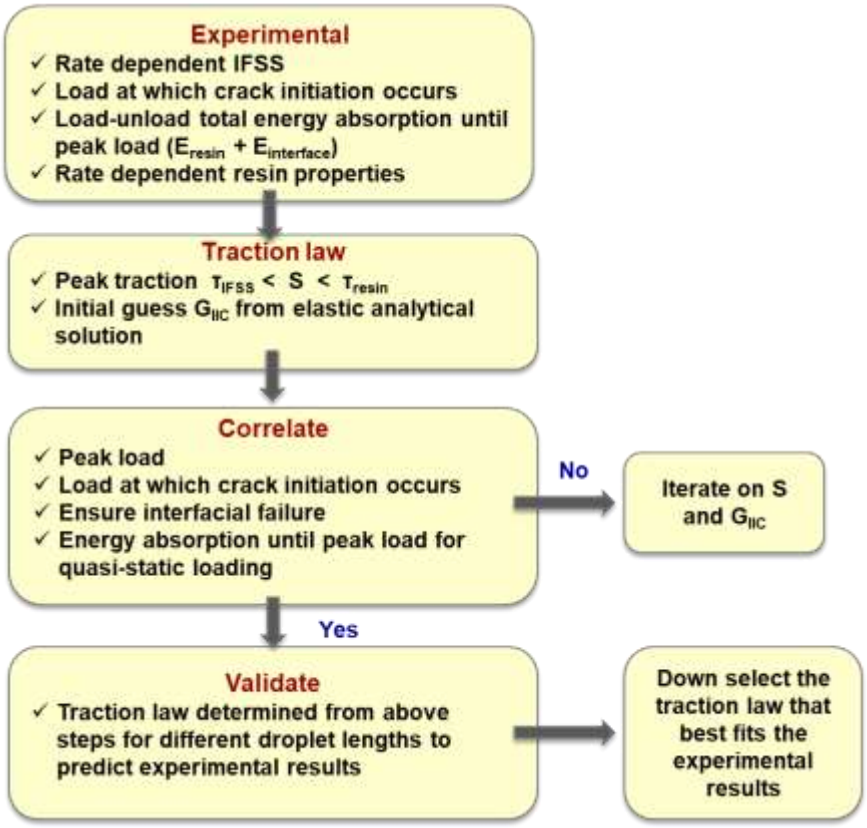

Figure 2 Methodology for determination of traction separation law for composite interface

The first step is to conduct the microdroplet experiments under different loading rates (Figure 2). During the experiment, cured specimens are placed on a specimen holder, which is attached to a load cell. Knife edges induce compression in the resin droplet resulting in large local deformation. This force is transferred to the fiber through shearing shear of the resin of and the interface, which results in the fiber being loaded in tension and is measured by the load cell.

In our methodology, we create specimens with a minimum of three embedded lengths (75 µm, 100 µm and 125 µm). We ensure that the failure mode is along the interface and not within the resin. Our study using CNT sensors indicate that the interface debonding occurs at the maximum load in our S glass/epoxy specimens [17]. The IFSS data for each embedded length is used to correlate with the numerical predictions.

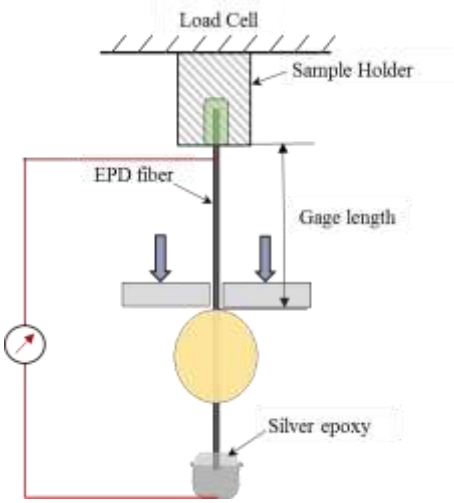

Figure 3 Quasi-static microdroplet test setup

A bilinear traction separation law is assumed for the interface under Mode II loading. The key parameters associated with the traction law are the peak shear stress (S) and the critical energy release rate, G_{IIc} (the critical shear displacement is calculated using the other parameters). It is important to note that the IFSS is an average value and that there is significant gradients along the droplet interface (highest near the knife-edge loading surface). Hence, IFSS is much lower than the peak shear stress defined in the traction law.

The simulation based iteration process using known properties of the fiber and epoxy resin begins by choosing a value for peak traction that is equal or higher than the average interfacial shear strength. Since the failure mode is confirmed experimentally to debond within the interphase, the peak stress should also not significantly exceed the yield stress of the resin (otherwise failure will occur in the resin and not be consistent with interfacial failure mode). Initial estimates for the critical energy release rate is calculated by using the critical opening displacement from the previous studies by Sockalingam et al. [13] assuming an elastic resin response for the same S glass (GPS sized)/epoxy constituents.

Simulations with different combinations of peak traction and critical energy release rate within this range are carried out for a 75 μm droplet. Combinations that cannot reach the maximum load are eliminated. Those combinations that match the peak experimental load are then checked for failure mode (interfacial or resin). Resin failure modes (extensive resin plasticity near the interface) and the associated traction law parameters are also eliminated. This sequence significantly narrows the range of admissible parameters.

This range of acceptable traction law parameters are then used to predict the IFSS for the next larger droplet sizes (100 μm and then 125 μm). This sequence is repeated and further narrowing of the range is achieved. Three drop sizes provide convergence of the traction law parameters that provides the correct failure mode and failure loads for all embedded lengths. The simulation results

also allow the partitioning of energy absorbing mechanisms (interface and resin plasticity) and prediction of cohesive zone sizes for all loading rates. Incorporating resin plasticity ensures energy absorption of the interface softening is accurate. Assuming elastic response (for a resin with extensive resin plasticity) will result in an overestimation of the interfacial energy absorption.

This procedure also works well for droplets tested at higher rates of loading, where only the maximum load can be measured accurately. This methodology provides a unique critical peak shear stress and energy absorption parameters for the Mode II traction law as a function of loading rate that can be used in other micromechanical simulations [18].

4. Finite element model

A quarter-symmetric FE Model was used to simulate the microdroplet experiment. S glass fiber (10 μm diameter), steel knife blade and epoxy resin droplet (with spherical shape) were modeled using 8-noded linear reduced-integration 3D Brick elements (C3D8R in ABAQUS), with enhanced hourglass control. Zero-thickness 3D cohesive elements (COH3D8) represent the fiber-matrix interface. The thermal preload during the curing of the droplet was modeled as an initial quasi-static step [13], while the subsequent knife edge loading was simulated as a dynamic explicit load step and solved using the double-precision ABAQUS Explicit solver.

The fiber is modeled as isotropic linear elastic material. The matrix is modeled isotropic linear elastic up to yield. Rate dependent post yield behavior of the epoxy resin obtained from compression experiments serves as model input. The resin exhibits post yield softening, plastic flow followed by strain hardening at large strain. Element deletion occurs at the failure strain of 70%. Input properties of fiber and matrix can be found in [17]. Post yield stress strain curve for 0.001/s strain rate is used. For higher strain rates, the entire curve is shifted vertically using the strain rate dependent yield stress. Details on curve fitting and yield stress prediction using Eyring equation are presented in our previous work [16]. Details regarding meshing and boundary conditions in the model can be found elsewhere [17].

Table 2 Properties of fiber and matrix

Property	S-glass fiber	Epoxy resin DER 353
Young's modulus (GPa)	90.0	3.2
Poisson's ratio	0.17	0.36
CTE (ppm/ºC)	3.4	70.0

5. Determination of traction separation law

5.1. High rate loading

For high loading rate of 1 m/s, the average IFSS for a 75 µm droplet was 88 MPa. So, a peak traction greater than 88 MPa was chosen based on our methodology. A series of parametric studies were conducted for a droplet with 75 µm embedded length to generate a family of IFSS vs. peak traction and fracture energy curves (Figure 4). In general, simulations with lower peak tractions showed delayed crack initiation at interface and higher peak traction showed resin failure. This trend is consistent with all the loading rates used in this study.

For 1 m/s, peak tractions ranging from 110 MPa to 150 MPa match the experimental IFSS and failure modes are carried forward to predict the IFSS for different droplet sizes as part of the procedure. Traction parameters that do not predict the experimental peak loads or failure modes are eliminated.

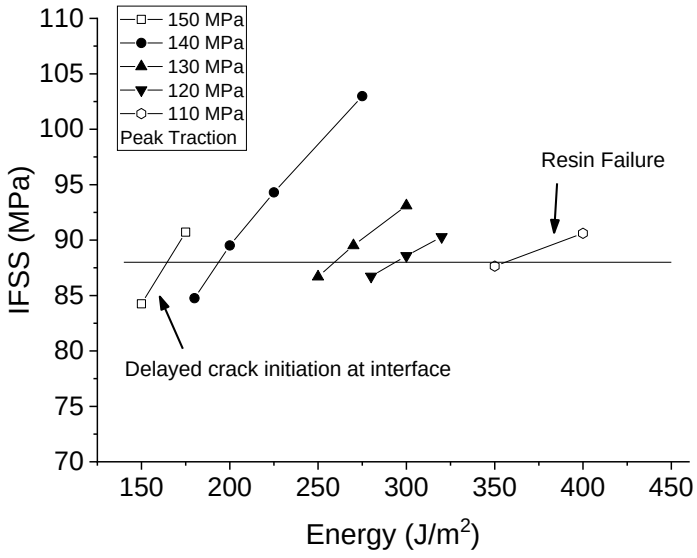

Figure 4 Parametric study on peak traction and fracture energy for the determination of traction separation law for 75 µm droplet at 1 m/s loading rate. Traction laws with peak shear stress of 110 MPa and 150 MPa are eliminated

Traction laws (120 MPa-300 J/m^2 and 130 MPa-270 J/m^2) exhibited correct failure modes for both 100 µm and 125 µm droplets. Size effects on the interfacial shear strength was also observed from simulation results (consistent with experimental observations), where larger droplet sizes showed lower IFSS. The traction law 120 MPa - 300 J/m^2 results in less error compared to the line fit to the experimental results. Hence this combination is chosen as the unique parameters for the loading

rate of 1 m/s. It should be noted that our methodology to determine unique traction separation law is limited by the variability in experimental data.

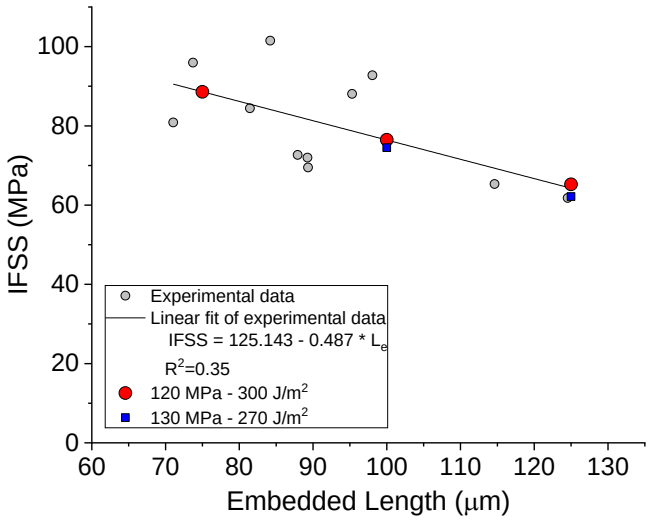

Figure 5 Average interfacial shear strength from microdroplet experiments and FE model showing size effects for 1 m/s loading rate

Table 3 Goodness of fit for the predicted IFSS at 1 m/s

Traction law	Error*
120 MPa and 300 J/m^2	0.54 %
130 MPa and 270 J/m^2	1.95 %

*$Error = \left|\frac{IFSS_{exp} - IFSS_{model}}{IFSS_{exp}}\right| \times 100\ \%$

5.2. Intermediate loading rate

For the intermediate loading rate of 100 μm/s microdroplet tests, the IFSS was 61 MPa for a nominal 75 μm droplet. Following the methodology, results from a parametric study done with peak traction ranging from 70 MPa to 90 MPa with a wide range of fracture energies are shown in Figure 6. For peak traction between 75 MPa and 85 MPa, failure occurred along the interface and the traction laws 75 MPa – 120 J/m^2, 75 MPa – 150 J/m^2, 80 MPa – 100 J/m^2, 80 MPa – 120 J/m^2 and 85 MPa and 90 J/m^2 predicted IFSS within the experimental error. However, when the peak traction of 70 MPa and 90 MPa exhibited delayed crack initiation at the interface and resin failure, respectively. Following our methodology, the traction law was narrowed down to 75 MPa – 150 J/m^2, which showed interfacial failure for both 75 μm and 125 μm droplets. Comparison of the simulation with the linear fit to the experimental results show an excellent correlation including size effect with an average absolute relative error of 5.9%.

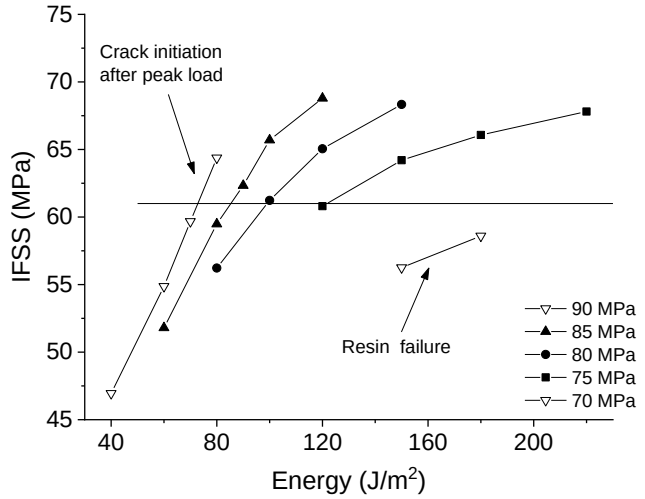

Figure 6 Parametric study on peak traction and fracture energy for the determination of traction separation law for 75 µm droplet at 100 µm/s loading rate

5.3. Quasi-static loading rates

For quasi-static loading rate of 1 µm/s, the average IFSS for a 75 µm droplet was 54 MPa. Traction laws with peak traction 60 MPa did not reach the experimental IFSS (Figure 7). The ones that matched the experimental IFSS (65 MPa - 100 J/m^2 and 70 MPa – 80 J/m^2) are carried forward and used to predict the IFSS for different droplet sizes.

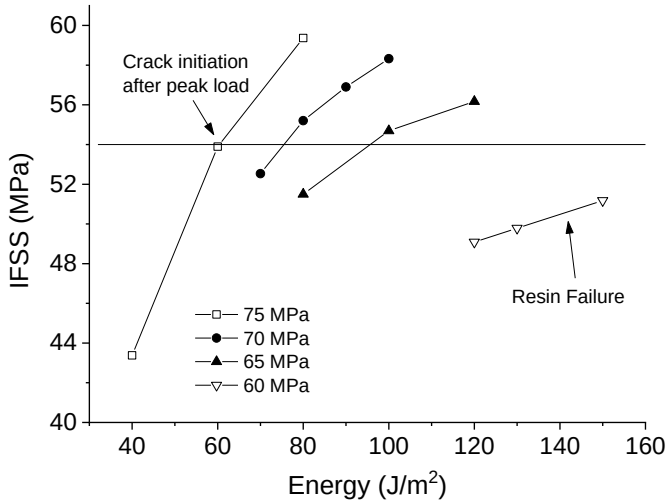

Figure 7 Parametric study on peak traction and fracture energy for the determination of traction separation law for 75 μm droplet at 1 μm/s loading rate. Traction laws with peak traction 60 MPa and 75 MPa are eliminated from further study

Simulations run with 70 MPa traction law exhibited delayed crack growth at the interface for droplet size of 125 μm and consequently was eliminated from further analysis. The FE predictions using the downselected traction law 65 MPa – 100 J/m^2 are within 2.9% of the line fit to the experimental data (Table 4).

Table 4 Goodness of fit for the predicted IFSS at 1 μm/s

Traction law	Error
65 MPa and 100 J/m^2	2.9 %
70 MPa and 80 J/m^2	5.1 %

6. Conclusions

A methodology has been developed to extract the rate dependent traction separation law for composite interface through iterative method by simulating microdroplet experiment. Experimental results show the interfacial properties are dependent on rate of loading and on the geometry of the specimen. Rate dependent inelastic resin properties were considered, which is critical for accurate determination of traction law. Use of only elastic properties for resin droplet tend to overestimate the traction law parameters of the interface. Crack initiation occurs at peak load, which correlates well with the experimental results obtained from CNT sensors. A range of traction separation laws were determined for different loading rates by simulating the microdroplet experiments with a certain embedded length. Then, unique rate dependent traction laws were determined by narrowing down the range by simulating microdroplets with different droplet sizes. The simulations showed a general trend where a lower peak traction exhibited resin failure and higher peak traction showed a brittle failure. These failure modes are associated with the crack opening displacements assumed in the traction law. These results showed the overall energy absorption capability and failure modes depend on the rate dependent peak traction stress and resin yield stress. Interfacial traction separation laws (both peak traction and the fracture energy) were found to be dependent on the rate of loading (Figure 8 and Table 5). The range of shear strain rates presented in Table 5 have been calculated by assuming interface thickness of 10 – 100 nm. Peak traction and fracture energy exhibit a fairly linear relation with shear strain rate when plotted on a semi log scale (Figure 9).

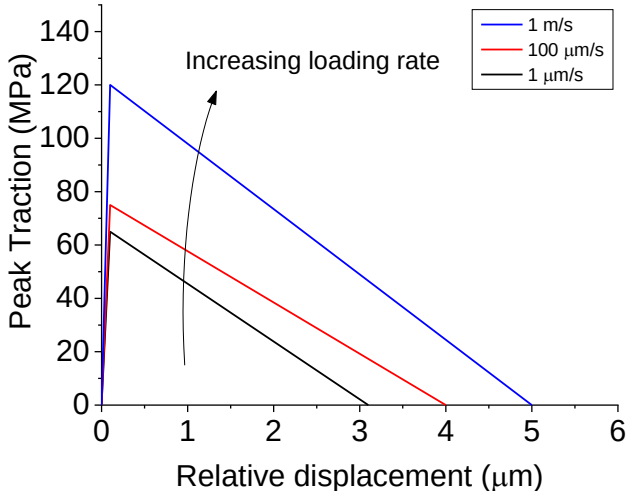

Figure 8 Traction separation law for different loading rates

Table 5 Rate dependent traction separation laws

Loading rate	Relative nodal velocity	Shear strain rate range	Peak traction	Fracture energy	Relative displacement
1 μm/s	0.9 μm/s	9/s – 90 /s	65 MPa	100 J/m^2	3.1 μm
100 μm/s	90 μm/s	900/s – 9000/s	75 MPa	150 J/m^2	4.0 μm
1 m/s	1 m/s	10^7 /s - 10^8 /s	120 MPa	300 J/m^2	5.0 μm

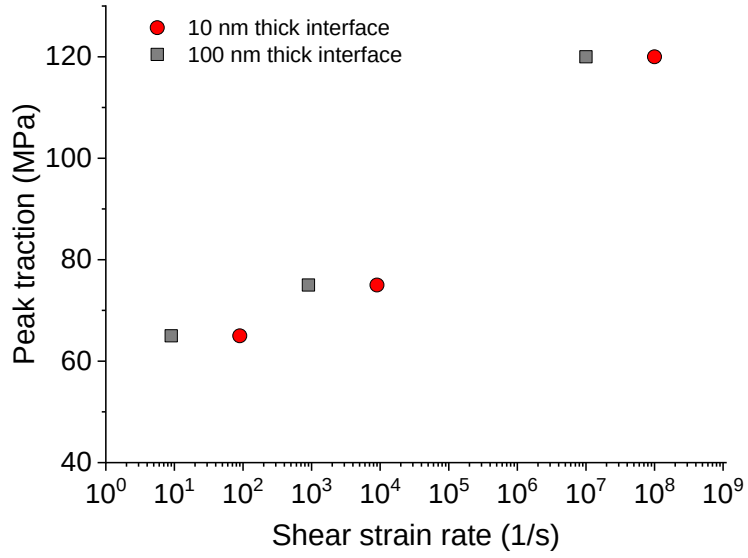

(a)

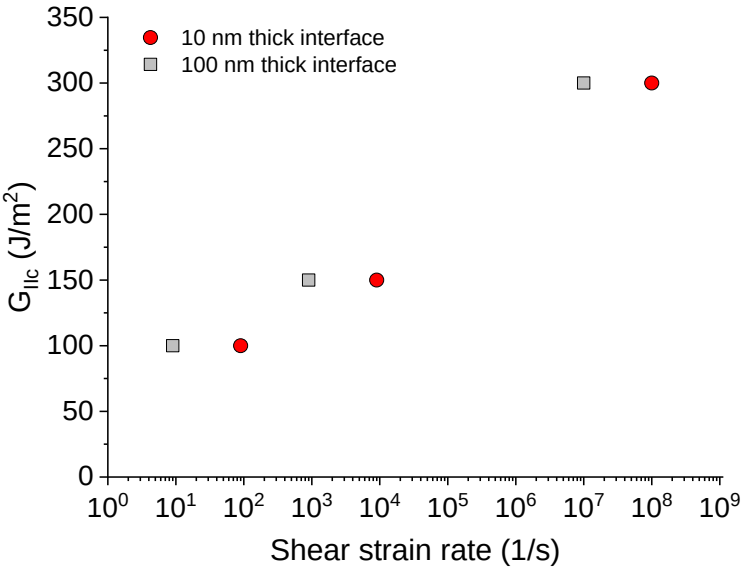

(b)

Figure 9 (a) Peak traction and (b) fracture energy as a function of shear strain rate for interface with 10 nm and 100 nm thickness

7. Acknowledgements

Research was sponsored by the Army Research Laboratory and was accomplished under Cooperative Agreement Number W911NF-12-2-0022. The views and conclusions contained in this document are those of the authors and should not be interpreted as representing the official policies, either expressed or implied, of the Army Research Laboratory or the U.S. Government. The U.S. Government is authorized to reproduce and distribute reprints for Government purposes notwithstanding any copyright notation herein.

8. References

[1] J. Kim, Y. Mai, Engineered interfaces in fiber reinforced composites, First Edit, Elseview Science Ltd, 1998. http://books.google.com/books?hl=en&lr=&id=qrjC9Yt8y6kC&oi=fnd&pg=PP2&dq=Engineered+interfaces+in+Fiber+Reinforced+Composites&ots=G3SFmO3Kg7&sig=F1ilVP4gIogQ9W17uwdoFJ0SCm4 (accessed November 4, 2013).

[2] M. Tanoglu, Investigation of the fiber/matrix interphase under high loading rates, Unviersity of Delaware, 2000.

[3] X. Gao, J.W. Gillespie, R.E. Jensen, W. Li, B.Z. (Gama) Haque, S.H. McKnight, Effect of fiber surface texture on the mechanical properties of glass fiber reinforced epoxy composite, Compos. Part A Appl. Sci. Manuf. 74 (2015) 10–17. doi:10.1016/j.compositesa.2015.03.023.

[4] M. Dey, J.M. Deitzel, J.W. Gillespie, S. Schweiger, Influence of sizing formulations on glass/epoxy interphase properties, Compos. Part A Appl. Sci. Manuf. 63 (2014) 59–67. doi:10.1016/j.compositesa.2014.04.006.

[5] X. Gao, R.E. Jensen, S.H. McKnight, J.W. Gillespie, Effect of colloidal silica on the strength and energy absorption of glass fiber/epoxy interphases, Compos. Part A Appl. Sci. Manuf. 42 (2011) 1738–1747. doi:10.1016/j.compositesa.2011.07.029.

[6] K. Park, G.H. Paulino, Cohesive Zone Models: A Critical Review of Traction-Separation Relationships Across Fracture Surfaces, Appl. Mech. Rev. 64 (2013) 060802. doi:10.1115/1.4023110.

[7] S. Gowrishankar, H. Mei, K.M. Liechti, R. Huang, A comparison of direct and iterative methods for determining traction-separation relations, Int. J. Fract. 177 (2012) 109–128. doi:10.1007/s10704-012-9758-3.

[8] Y. Zhu, K.M. Liechti, K. Ravi-Chandar, Direct extraction of rate-dependent traction–separation laws for polyurea/steel interfaces, Int. J. Solids Struct. 46 (2009) 31–51. doi:10.1016/j.ijsolstr.2008.08.019.

[9] P. Rahulkumar, A. Jagota, S.J. Bennison, S. Saigal, Cohesive element modeling of viscoelastic fracture: application to peel testing of polymers, Int. J. Solids Struct. 37 (2000) 1873–1897. doi:10.1016/S0020-7683(98)00339-4.

[10] C. Xu, T. Siegmund, K. Ramani, Rate-dependent crack growth in adhesives: I. Modeling approach, Int. J. Adhes. Adhes. 23 (2003) 9–13. doi:10.1016/S0143-7496(02)00062-3.

[11] J. Wang, Q.H. Qin, Y.L. Kang, X.Q. Li, Q.Q. Rong, Viscoelastic adhesive interfacial model and experimental characterization for interfacial parameters, Mech. Mater. 42 (2010) 537–547. doi:10.1016/j.mechmat.2010.03.002.

[12] S. Marzi, O. Hesebeck, M. Brede, F. Kleiner, A Rate-Dependent Cohesive Zone Model for Adhesively Bonded Joints Loaded in Mode I, J. Adhes. Sci. Technol. 23 (2009) 881–898. doi:10.1163/156856109X411238.

[13] S. Sockalingam, M. Dey, J.W. Gillespie, M. Keefe, Finite element analysis of the microdroplet test method using cohesive zone model of the fiber/matrix interface, Compos. Part A Appl. Sci. Manuf. 56 (2014) 239–247. http://www.sciencedirect.com/science/article/pii/S1359835X13002960 (accessed November 22, 2013).

[14] B.N. Cox, D.B. Marshall, The determination of crack bridging forces, Int. J. Fract. 49 (1991) 159–176. doi:10.1007/BF00035040.

[15] S. Tamrakar, B.Z. Haque, J.W. Gillespie, High rate test method for fiber-matrix interface characterization, Polym. Test. 52 (2016) 174–183. doi:10.1016/j.polymertesting.2016.04.016.

[16] S. Tamrakar, R. Ganesh, S. Sockalingam, B.Z. Haque, J.W. Gillespie, Experimental Investigation of Strain Rate and Temperature Dependent Response of an Epoxy Resin Undergoing Large Deformation, J. Dyn. Behav. Mater. 4 (2018) 114–128. doi:10.1007/s40870-018-0144-8.

[17] S. Tamrakar, Characterization of S-glass epoxy composite interface under various rates of loading, University of Delaware, 2018.

[18] R. Ganesh, S. Sockalingam, B.Z. (Gama) Haque, J.W. Gillespie, Dynamic effects of single fiber break in unidirectional glass fiber-reinforced composites, J. Compos. Mater. 51 (2017) 1307–1320. doi:10.1177/0021998316669218.